MINERALOGICAL MAGAZINE, JUNE 1985, VOL. 49, PP. 435-449

Hydrothermal mineralogy of calcareous sandstones from the Colorado River delta in the Cerro Prieto geothermal system, Baja California, Mexico

PETER SCHIFFMAN,[1,2] DENNIS K. BIRD,[3] AND WILFRED A. ELDERS[1]

ABSTRACT. The Cerro Prieto geothermal system provides a unique opportunity for the detailed study of calc-silicate mineral transitions between the diagenetic clay–carbonate and greenschist facies within the terrigenous sediments of the Colorado River delta. In this system, progressive devolatization reactions within carbonate-cemented, quartzofeldspathic sediment have produced a distinct hydrothermal mineral zonation at temperatures between 200–370 °C and fluid pressures below 0.3 kbar. Descriptive and compositional data are presented for these minerals which include wairakite, epidote, prehnite, actinolite, clinopyroxene, garnet, sphene, biotite, microcline, and calcite. Partitioning of octahedral Fe, Mg, and Al between coexisting authigenic silicates is comparable with data from higher temperature metamorphic rocks and demonstrates an approach to local equilibrium within this system. Calculated fugacities of oxygen at temperatures above 300 °C are (with rare exception) more reducing than that defined by the quartz–fayalite–magnetite buffer, a result consistent with the scarcity of hematite and grandite and the ubiquitous presence of organic material in Cerro Prieto sandstones.

KEYWORDS: sandstones, geothermal system, wairakite, epidote, prehnite, actinolite, clinopyroxene, biotite, sphene, garnet, microcline, Cerro Prieto, Mexico.

IN recent years, mineralogical and geochemical studies of rock samples from oil and gas wells have afforded considerable insights into the diagenetic recrystallization of argillaceous sedimentary detritus (e.g. see articles in Scholle and Schluger, 1979). In an analogous fashion, samples recovered from wells in active geothermal systems provide a unique opportunity for the *in situ* investigation of low-pressure hydrothermal metamorphism. Moreover, as geothermal systems are developed in reservoirs characterized by a broad spectrum of potentially well-defined physical and chemical parameters, they provide natural laboratories for the study of the hydrothermal recrystallization of most metamorphic rock protoliths.

The Cerro Prieto geothermal system is one of the most intensively studied and best characterized geothermal fields in the world. We have previously reported on various aspects of the petrology and geochemistry of this system; its unique metamorphic mineral zonation (Schiffman *et al.*, 1984), the thermodynamic relationships between minerals and hydrothermal fluids (Bird *et al.*, 1984), and the relationship between fluid flow and possible magmatic heat sources (Elders *et al.*, 1984). In the present paper, we describe the mineralogy and mineral chemistry of recrystallized calcareous sediments and their relationships to known physical conditions of metamorphism in this system. Ever since the pioneering works of Harker (1932) and Bowen (1940), metamorphic petrologists have been attempting to delineate carefully the physical and chemical conditions attending the recrystallization of calcareous sediments. By combining experimental, analytical, and theoretical approaches, our understanding of the petrogenesis of these rocks, particularly at higher metamorphic grades, has dramatically increased in the past few decades (e.g. see discussion in Rice and Ferry, 1982). Observing recrystallization of calcareous sediments in an active geothermal system offers yet another perspective, especially in elucidating the transitions between diagenetic and truly metamorphic mineral parageneses.

Calcareous sediments of the Cerro Prieto geothermal system

The Cerro Prieto geothermal field (fig. 1), 28 km southeast of Mexicali, Mexico, is underlain by deltaic sediments of the Colorado River at the head of the Gulf of California. Since the Pliocene or late Miocene terrigenous sediments of the Colorado River have been deposited into the Salton Trough

[1] Institute of Geophysics and Planetary Physics, University of California, Riverside, California 92521 USA.

[2] Department of Geology, University of California, Davis, California 95616 USA.

[3] Department of Geology, Stanford University, Stanford, California 94305 USA.

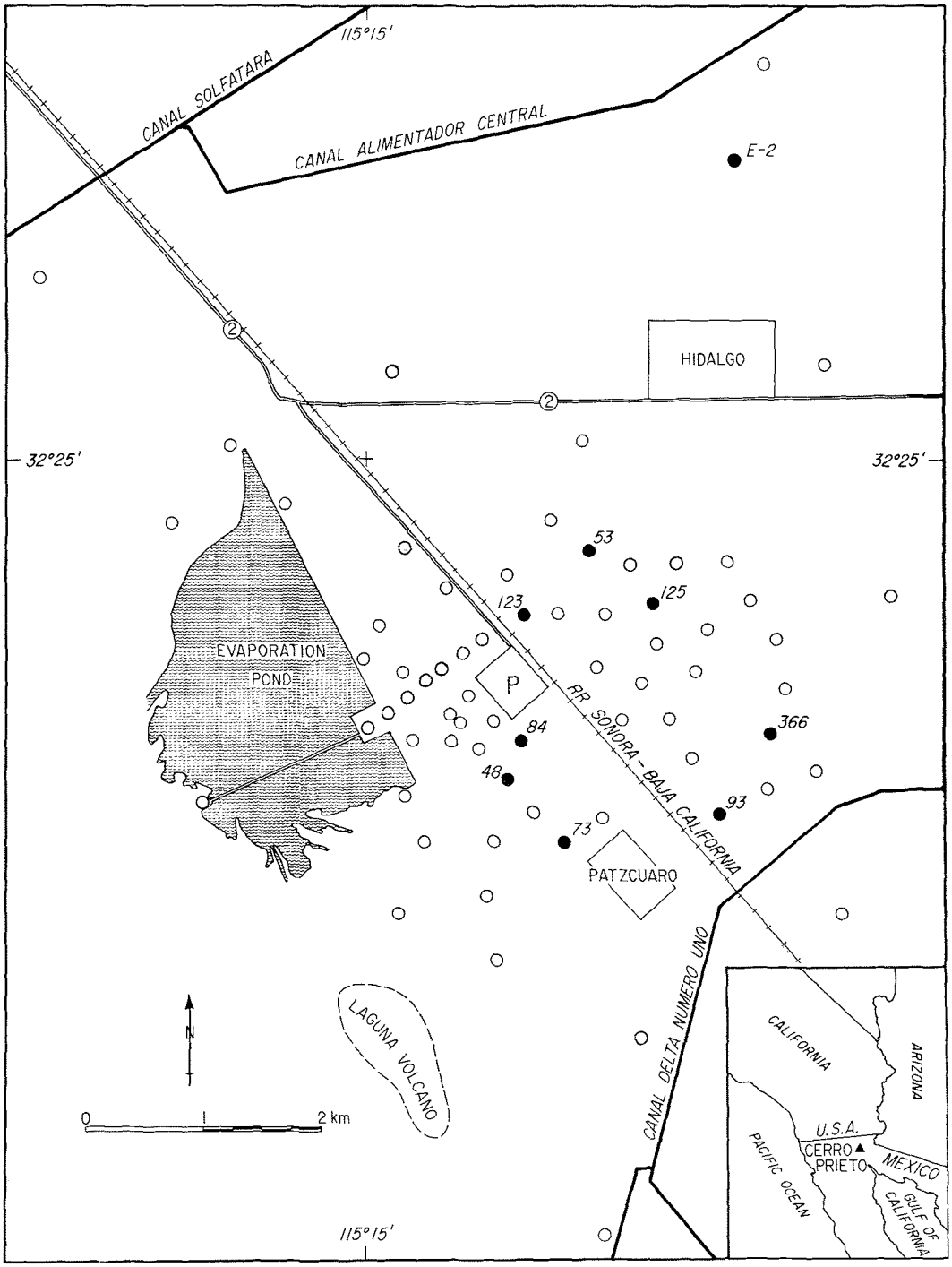

FIG. 1. Sketch map of the Cerro Prieto geothermal field, Baja California, Mexico. Circles indicate existing wells; wells from which samples have been analysed for this study are numbered. P = power plant, Cerro Prieto 1.

(Muffler and White, 1969; Van de Kamp, 1973), a large structural basin in which many active geothermal systems are developed. Stratigraphic thicknesses of deltaic sediments in the Salton Trough are believed to approach 6 km (Muffler and Doe, 1968). Seismic stratigraphy (Fuis *et al.*, 1982) indicates a two-layer regional crustal structure: an upper section, approximately 5 km thick whose seismic properties (V_p = 2 to 5.6 km/sec) are compatible with unmetamorphosed sediments, and a 10 km lower section characterized by a constant V_p = 5.65 km/sec, compatible with metamorphosed sediments. In the Cerro Prieto geothermal field, wells in excess of 3 km have not reached basement, although thermal modelling (Elders *et al.*, 1984) indicates that the sediments are probably underlain by a large gabbroic intrusive body which is responsible for the thermal anomaly.

Unmetamorphosed sediments in the Cerro Prieto geothermal field are compositionally akin to modern deltaic Colorado River sediments (Muffler and Doe, 1968) and to other unmetamorphosed sediments of the Salton Trough (Van de Kamp, 1973). They consist largely of continentally derived sandstones, siltstones, and mudstones predominantly comprised of quartz and feldspar with subordinate amounts of carbonate (both calcite and dolomite) and clays (illite, smectite, and kaolinite). Also present are minor quantities of heavy minerals and detrital phyllosilicates (i.e. muscovite, biotite, and chlorite), lithic fragments (predominantly chert and volcanic), and organic material such as lignite and vitrinite macerals (Barker and Elders, 1981).

Within the Cerro Prieto geothermal field, sandstones, siltstones, and mudstones are intimately interbedded, locally on centimetre scale. Bulk X-ray diffraction analysis (Elders *et al.*, 1979) of the least recrystallized sediments at the top of the reservoir indicate that in general: (1) sandstones contain nearly twice as much detrital quartz as do the contiguous mudstones (i.e. approximately 50–60% versus 25–30%); (2) sandstones and mudstones have roughly the same detrital alkali feldspar and plagioclase contents (i.e. generally 3–10% of each); and (3) mudstones are greatly enriched in detrital (and possibly authigenic) kaolinite, illite, and smectite relative to sandstones (i.e. 40% versus 5%). The metamorphic mineralogy observed in mudstones and siltstones is roughly similar to that described below for sandstones, although any given mineral isograd (Schiffman *et al.*, 1984) occurs at higher temperatures in mudstones than in sandstones, possibly due to the effects of permeability on the metasomatic reactions (Elders *et al.*, 1979). We have concentrated our efforts on sandstone cuttings for analytical expedience.

Induration of sediments within the Cerro Prieto field occurs in response to post-depositional development of either low temperature (i.e. < 200–250 °C) cements consisting predominantly of carbonate with subordinate silica, potassium feldspar, pyrite, and layer silicates, or to higher temperature (i.e. > 200–250 °C) pore-filling calc-silicate assemblages, typical of low-grade metamorphic rocks (see below). Shallow sediments which overlie the geothermal reservoir are unconsolidated and were incompletely recovered during drilling. Carbonate cementation develops at the top of the reservoir presumably due to the heating of shallow groundwater which decreases the solubility of dissolved carbonate, some of which may be derived by upward migration of CO_2 evolved from reservoir rocks which are undergoing devolatization at higher temperatures. Carbonate cementation first occurs at depths ranging from 500 to 2000 m and at temperatures between 50 and 100 °C. X-ray diffraction analysis (Elders *et al.*, 1979) indicate that these lowest-temperature carbonate cements are predominantly dolomitic with subordinate calcite and that in cuttings from the temperature interval of 100 to 250 °C, calcite replaces dolomite as the major carbonate cement with detrital (possibly also authigenic) smectite and kaolinite replaced by authigenic illites, illite–smectite, and chlorite (Elders *et al.*, 1979). However, the details of these lower temperature phyllosilicate transformations have not been fully investigated.

Calcite cemented sandstones within the so-called 'carbonate-cap' rocks of the geothermal reservoir have extremely low porosities (Elders *et al.*, 1984). Thus, this horizon which may be several hundred metres thick (see fig. 3 of Schiffman *et al.*, 1984) forms an effective permeability barrier to the geothermal reservoir. It is the dissolution of this carbonate cement, which generally first occurs at temperatures in excess of 200 °C, that marks the onset of the calc-silicate mineral zones: wairakite (at 200 °C), epidote (at 230 °C), prehnite–actinolite (at 270 °C), and clinopyroxene–biotite (at 320 °C). Details of the calc-silicate mineral zones and their isogradal relations are presented in Schiffman *et al.* (1984).

Inception of the calc-silicate zone marks a pronounced change in the nature of the cementation. The earlier-formed carbonate cement (fig. 2*a*) is gradually replaced by calc-silicate cements (fig. 2*b–d*). These minerals nucleate and grow predominantly within and at the expense of the carbonate cement, and only partially (with the exception of microcline) replace the framework grains (i.e. feldspar and quartz). In sandstone samples from the highest temperature parts of the geothermal reservoir (e.g. those which contain

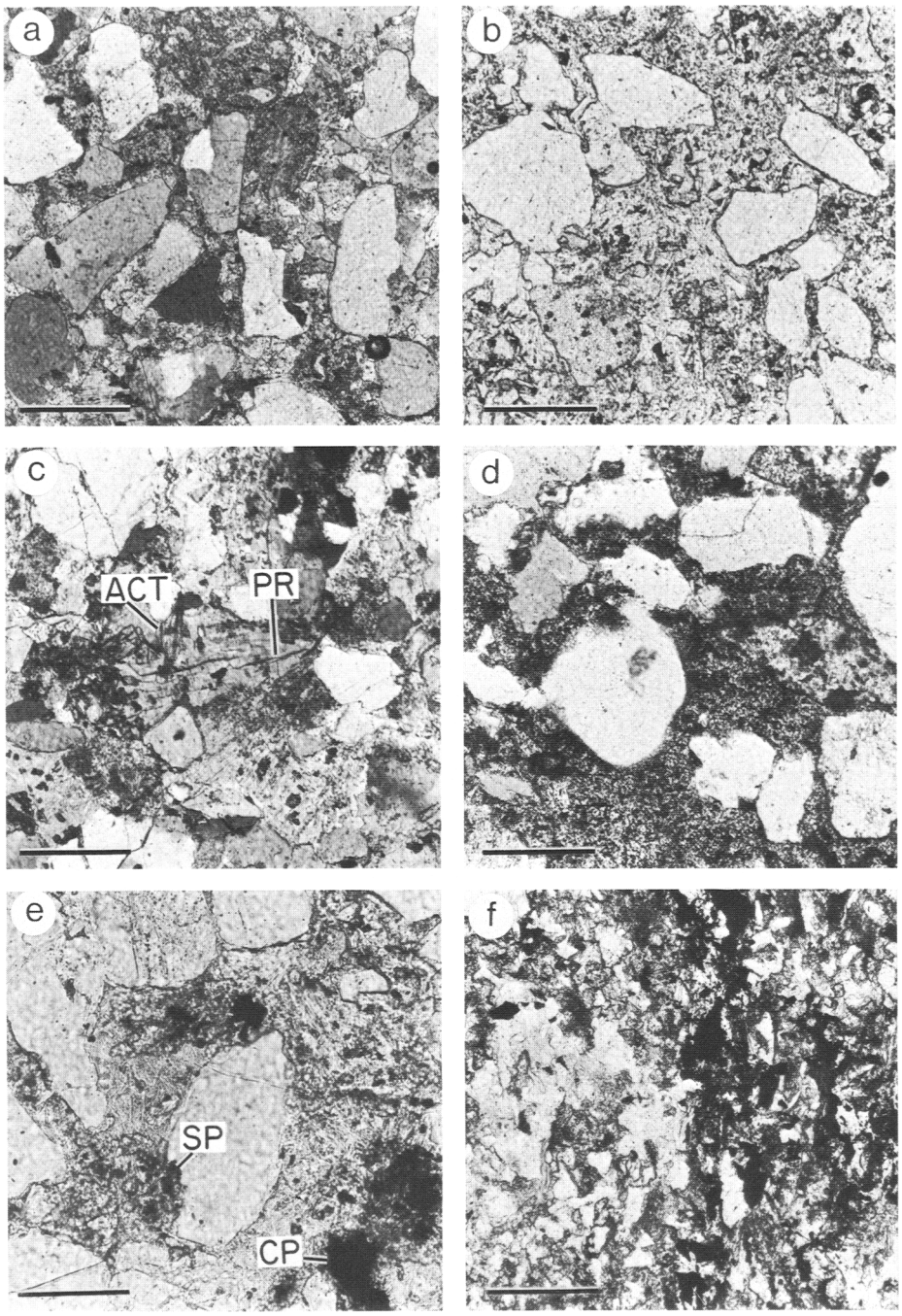

FIG. 2. Calcareous sandstones of the Cerro Prieto geothermal system. (*a*) calcite cemented sandstone from well M84, 1086 m depth, partially crossed polarizers, scale bar = 0.11 mm; (*b*) epidote cemented sandstone from well M93, 2424 m depth, plane polarized light, scale bar = 0.09 mm; (*c*) prehnite-cemented sandstone from well M84, 1557 m depth, partially crossed polarizers, scale bar = 0.07 mm; (*d*) clinopyroxene-cemented sandstone from well M93, 2424 m depth, plane-polarized light, scale bar = 0.08 mm; (*e*) porous sandstone with acicular matrix actinolite and clinopyroxene and granular sphene and chalcopyrite from well M73, 1890 m, plane polarized light, scale bar = 0.04 mm; (*f*) lignite-rich, thinly bedded sandstone from well E2, 1680 m, plane polarized light, scale bar = 0.09 mm; abbreviations are pr = prehnite, act = actinolite, sp = sphene, cp = chalcopyrite.

clinopyroxene), grain boundaries between pore-filling calc-silicates and detrital framework grains are often readily apparent (fig. 2*d*). Textural variations through these mineral zones are largely restricted to the pore-filling cement. Framework silicate grains undergo some resorption, replacement, or overgrowth and matrix phyllosilicates are progressively recrystallized, but the major textural and mineralogical modification of these sediments occurs in the pore-filling cement and in fractures.

Hydrothermal mineralogy

In the Cerro Prieto geothermal system, hydrothermal minerals include wairakite, microcline, epidote, prehnite, actinolite, clinopyroxene, biotite, garnet, and sphene. These minerals occur as coarser grained pore-filling cements (i.e. wairakite, epidote, prehnite, and clinopyroxene; fig. 2*b*, *c*, and *d*), finer grained authigenic matrix (i.e. actinolite, biotite, clinopyroxene, garnet, and sphene; figs. 2*e*, 3*d*, *e*, and *f*), and within veins which are often zoned (fig. 3*a*, *b*, and *c*) and may be comprised of all the above mentioned minerals except biotite and garnet.

Representative compositions of Cerro Prieto metamorphic minerals are presented in Tables I–VII. Electron microprobe analyses entailed both wavelength dispersive (WDS) and energy dispersive (EDS) spectrometric techniques. WDS analyses were conducted on a M.A.C.5-SA3 microprobe operated at 15 keV and sample currents of 5 or 50 nA; data were reduced using Bence–Albee (1968) standards and correction techniques employing the alpha factors from Albee and Ray (1970). Most EDS analyses were conducted on an A.R.L.-EMX microprobe equipped with a Kevex 7000 spectrometer and operated at 15 keV and beam currents of 100 or 300 nA; data were corrected for Z.A.F. effects using Colby's (1968) Magic 5 technique. In Tables II–VII, oxide analyses of WDS analyses are reported to a precision of ± 0.01 wt. % and EDS analyses to ± 0.1 wt. %.

Calcite cements occur in a variety of grain sizes and textures ranging from microcrystalline to more coarsely crystalline mosaic (fig. 2*a*) and even poikiloblastic varieties. Compositionally (Table I), these cements comprise in excess of 97% $CaCO_3$, with subordinate $MgCO_3$, $FeCO_3$, and $MnCO_3$. Calcites in well M84 do not exhibit any systematic compositional changes over the temperature interval of 185–320 °C (Table I). X-ray diffraction analyses indicate that calcite modes decrease from > 15 to $< 5\%$ at temperatures $\geqslant 200$ °C due to decarbonization reactions that form calc-silicate and related minerals.

Wairakite first appears as a pore-filling cement in sandstones recrystallized at temperatures of 200 to 230 °C. Petrographically, sandstones which contain abundant wairakite cement have a distinctive 'dark' appearance when viewed under cross-polarized light, even if individual crystals are not discernable. Rare, coarse-grained (< 0.05 mm in max. diameter) wairakites are subidioblastic and exhibit characteristic lamellar twinning parallel to crystal faces. When present, these coarse-grained wairakites typically form in equigranular mosaic aggregates; wairakite forms almost exclusively as pore-filling cement or in veins (fig. 3*a*) and only rarely has it been observed as a replacement of detrital feldspars or lithic clasts. Compositionally, wairakite is close to being stoichiometric $Ca_2Al_2Si_4O_{12} \cdot 2H_2O$. Microprobe analyses (Table II) indicate that molar Ca(Na + K + Ca) ranges from 0.90 to 1.00 with a mean of 0.97 ± 0.03. K_2O is scarce (< 0.03 wt. %) although these wairakites invariably coexist with highly potassic, authigenic microcline.

Microcline, typically exhibiting well-developed cross-hatched twinning, accounts for 5–10% of sandstone modes in calc-silicate zone mineral assemblages. These feldspars apparently formed by recrystallization of detrital plagioclase and alkali feldspar framework grains. Representative analyses are presented in Table II. Compositionally, the microclines range from Or 91–97 with a mean near Or 95. No authigenic plagioclase feldspars have been petrographically identified in samples from the Cerro Prieto geothermal field although 'plagioclase' typically comprises between 0–10% of the sandstone mineral mode in quantitative XRD analysis (Elders *et al.*, 1979) in samples from all depths.

Epidote is the most abundant calc-silicate mineral in the Cerro Prieto geothermal field and occurs in veins (fig. 3*a*, *b*, *c*) and cement (fig. 2*b*) within sandstones and shales at temperatures > 230 °C. Radiating aggregates of fine-grained acicular crystals within carbonate pore-filling cement are characteristic of epidotes crystallized at temperatures slightly > 230 °C. At greater depths and temperatures (> 300 °C) epidotes are considerably coarser grained (< 0.5 mm in max. dimension), more prismatic, and texturally replace earlier formed calcite or wairakite. Interstitial epidote crystals are typically moulded about and partially embay the sub-rounded edges of detrital quartz or feldspar grains. Away from the boundaries of these grains, epidotes become subidioblastic and densely intergrown (fig. 2*b*). In a given sandstone/siltstone, epidote never exceeds the grain size of detrital silicate constituents. They are rarely porphyroblastic and never poikiloblastic. Epidotes from the Cerro Prieto geothermal field exhibit a substantial compositional range in solid solution

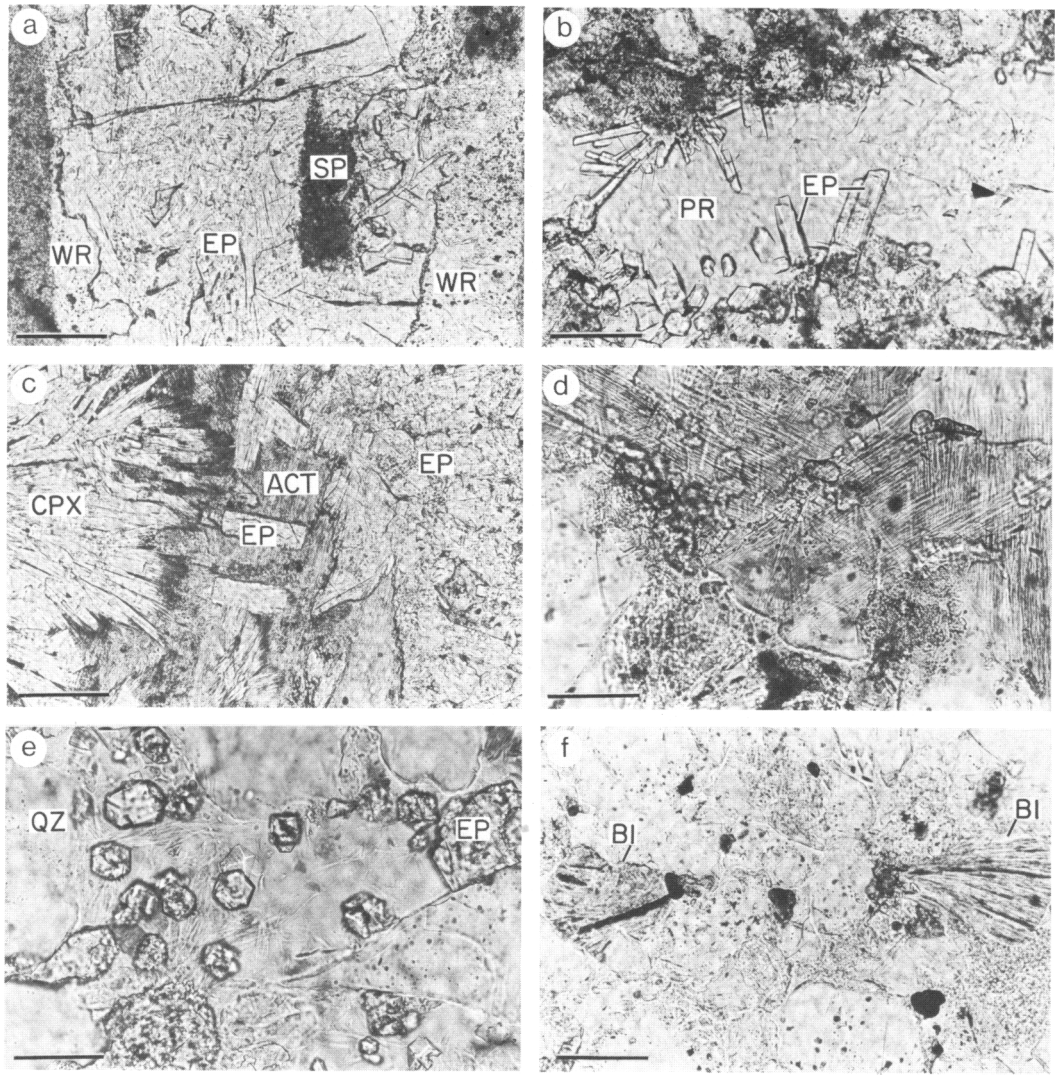

FIG. 3. Hydrothermal minerals from veins and sandstones in the Cerro Prieto geothermal system. (*a*) Epidote and sphene vein cutting earlier wairakite vein from well E2 at 1500 m depth, plane polarized light, scale bar = 0.04 mm; (*b*) epidote–prehnite vein from well E2 at 1500 m, plane polarized light, scale bar = 0.04 mm; (*c*) actinolite–clinopyroxene–epidote vein from well M73 at 1890 m, plane polarized light, scale bar = 0.04 mm; (*d*) fibrous actinolite aggregates in well M123 at 1704 m, plane polarized light, scale bar = 0.02 mm; (*e*) idioblastic garnet and subidioblastic epidote in matrix of porous sandstone from well E2 at 1581 m depth, plane polarized light, scale bar = 0.02 mm; (*f*) biotite aggregates in well M123 at 1704 m, plane polarized light, scale bar = 0.02 mm; abbreviations are wr = wairakite, ep = epidote, sp = sphene, act = actinolite, cpx = clinopyroxene, qz = quartz, bi = biotite, pr = prehnite.

with a pistacite (Ps, $Ca_2Fe_3Si_3O_{12}OH$) mole fraction between 11 to 31 % (Table III). Compositional zoning within individual crystals or between crystals from the same cutting chip (always separated by less than 5 mm) is generally less than 5 mol. % Ps.

Prehnite is a common phase in veins (fig. 3*b*) and an intergranular cement (fig. 2*c*) in sandstones at $> 270\,^{\circ}C$. Prehnite can comprise up to 20 % of the mode of sandstone samples, but more commonly $< 5\,\%$. In sandstone cuttings it invariably occurs as coarse-grained (up to 2 mm, but generally less than 1 mm, in max. dimension) xenoblastic poikiloblasts enclosing detrital framework grains (fig. 2*c*), and to a lesser extent, other pore-filling calc-silicates.

TABLE I. Compositions of carbonate cements in Cerro Prieto sandstones

Well #	Depth (m)	Temp.(1) (°C)	$MgCO_3$(2) (%)	$CaCO_3$ (%)	$MnCO_3$ (%)	$FeCO_3$ (%)
M84	990	185	0.6	98.5	0.5	0.4
M84	1086	250	0.2	96.8	0.6	2.4
M84	1299	320	0.1	99.5	0.3	0.1
M53	1935	330	0.4	98.4	0.8	0.4
M53	1974	335	1.2	97.3	0.7	0.8

(1) Downhole log temperature rounded to ±5 °C;

(2) Compositions expressed as molar cationic percents.

TABLE II. Compositions of wairakite and microcline from Cerro Prieto sandstones

	Wairakite(1)		Microcline(2)			
Well	M84	M53	M84	M93	M125	T366
Depth (m)	1284	1842	1299	2454	2241	2850
Temp(°C)	320	320	320	330	340	320
SiO_2	54.8	56.6	65.09	65.02	65.62	64.47
Al_2O_3	22.7	23.2	18.75	17.86	18.17	18.21
FeO(3)	0.1	0.0	0.20	0.20	tr	tr
CaO	12.8	12.7	0.00	0.00	0.00	0.00
K_2O	tr	0.1	15.92	16.05	14.72	15.77
Na_2O	bd	0.6	0.64	0.64	0.96	0.59
Total	90.4	93.2	100.56	99.74	99.47	99.24
Si	4.02	4.03	2.99	3.01	3.02	3.00
Al	1.94	1.95	1.00	0.98	0.98	1.00
Fe	0.00	0.00	0.01	0.01	0.00	0.00
Ca	1.01	.97	0.00	0.00	0.00	0.00
Na	0.00	0.09	0.06	0.06	0.09	0.06
K	0.00	0.01	0.93	0.95	0.86	0.93

(1) Wairakite formula proportions based on 12 oxygens; (2) microcline formula proportions based on 8 oxygens; (3) FeO as total iron; tr=Trace; (4) bd=Below detection limit.

TABLE III. Compositions of coexisting epidotes and prehnites from Cerro Prieto sandstones

	Epidote(1)								Prehnite(2)						
Well	M48	M84	M84	M93	M125	M125	T366	E2(4)	M48	M84	M84	M93	M125	M125	T366
Depth (m)	1199V(3)	1470	1557	2391	2019	2319	2985	1581	1199	1470	1557	2319	2019	2319	2985
Temp(°C)	325	335	340	325	350	335	325	325	325	335	340	325	350	335	325
SiO_2	37.23	38.41	38.18	38.88	37.43	38.15	37.62	36.9	41.83	44.03	42.74	42.94	42.15	42.77	42.76
Al_2O_3	24.03	25.64	24.95	25.29	25.83	26.44	25.31	22.4	21.43	23.63	23.93	23.64	22.76	23.31	23.36
Fe_2O_3	12.26	9.81	11.82	9.96	8.96	8.48	10.32	12.5	3.79	1.42	1.32	0.85	1.66	1.41	0.76
MnO	0.22	0.26	0.25	0.24	0.13	0.25	na	bd	0.14	0.16	0.00	0.12	0.01	0.01	0.44
MgO	0.18	0.46	0.16	na	na	na	na	bd	0.01	0.08	0.01	na	na	na	0.00
CaO	23.66	23.41	23.47	23.85	23.72	23.81	23.58	23.2	26.21	27.02	26.77	27.49	26.79	26.92	26.07
Total	97.58	97.99	98.83	97.22	96.07	97.13	96.83	95.0	93.51	96.34	94.77	95.04	93.37	94.42	93.39
Si	2.957	3.009	2.991	3.051	2.990	3.009	2.994	3.02	2.980	3.009	2.970	2.974	2.982	2.988	3.013
Al^{IV}	0.043	0.000	0.009	0.000	0.010	0.000	0.006	0.00	1.020	0.991	1.030	1.026	1.018	1.012	0.987
Al^{VI}	2.207	2.369	2.296	2.339	2.423	2.459	2.369	2.17	0.780	0.913	0.931	0.905	0.881	0.909	0.954
Mn	0.015	0.017	0.016	0.016	0.009	0.016	0.000	0.00	0.008	0.009	0.000	0.007	0.001	0.001	0.026
Fe	0.741	0.579	0.698	0.589	0.539	0.503	0.619	0.77	0.203	0.081	0.069	0.049	0.088	0.074	0.040
Mg	0.021	0.054	0.018	0.000	0.000	0.000	0.000	0.00	0.001	0.009	0.001	0.000	0.000	0.000	0.000
Ca	2.014	1.965	1.970	2.005	2.030	2.012	2.011	2.04	2.001	1.979	1.993	2.040	2.030	2.016	1.969
$Fe/(Fe+Al^{VI})$	0.251	0.196	0.233	0.201	0.182	0.169	0.207	0.26	0.204	0.081	0.069	0.052	0.093	0.075	0.039

(1) Epidote formula proportions based on 8 cations; (2) prehnite formula proportions based on 7 cations;
(3) V = Vein sample; (4) epidote coexisting with garnet (Table 7); na = not analyzed

These poikiloblasts typically exhibit characteristic 'bow tie' extinction. Prehnite compositions (Table III) show a wide range in octahedral iron substitution for aluminium from 0.01–0.28 mole fraction of $Ca_2Fe(AlSi_3)O_{10}OH_2$, although the majority of the prehnites contain < 0.125. Compositional variations within individual prehnite poikiloblasts are large with the mole fraction of $Ca_2Fe(AlSi_3)O_{10}OH_2$ for a vein prehnite in well M48 at 1199 m ranging from 0.059 to 0.279 with oscillatory zoning, whereas included and coexisting epidotes vary only from PS 20 to 25 mol. % of $Ca_2Fe_3Si_3O_{12}(OH)$.

Actinolite occurs in veins (fig. 3*c*) and in the matrix of sandstones recrystallized at temperatures above approximately 280 °C. Cerro Prieto amphiboles typically occur in coarse (0.5 mm), brown-tinted, feathery masses (fig. 3*d*) characterized by pervasive, closely spaced, parallel striations. These amphiboles, which comprise $< 1\%$ of the total mode of a given sandstone sample, appear to form through the replacement of pre-existing, pore-filling material such as calcite or detrital/authigenic phyllosilicate matrix. Most sandstones from the calc-silicate zone contain (secondary) pore space which is variably filled with mattes of randomly oriented, very fine-grained, acicular crystallites (fig. 2*e*). The optical properties of these crystallites (pale green to colourless, moderate (+) relief, and near parallel extinction) are compatible with either actinolite or chlorite, perhaps both. Rarely, these crystallites appear to grade perceptively into the coarser, brownish actinolitic aggregates described above. Representative analyses of Cerro Prieto amphiboles are presented in Table IV. Because of the fibrous and porous nature of most of these amphiboles, determined anhydrous oxide totals were often as low as 80%; therefore values for individual oxides are not given in Table IV. However, the stoichiometry of the recalculated cationic proportions as presented in Table IV attests to the reliability of these analyses. These amphiboles are all actinolites with minor formula proportions of Al, Na, Ti, and K. Mn is the only appreciable minor component on octahedral sites. Compositional zonation within individual actinolites or aggregates has not been observed.

Clinopyroxene, which crystallizes at temperatures in excess of 300 °C, occurs typically as subidioblastic prisms (< 0.2 mm in max. dimension) with well-developed {110} crystal faces and cleavage. These prismatic clinopyroxenes typically terminate into acicular projections elongate parallel to {110} (fig. 3) and occur exclusively as pore-filling cement or in veins. The pore-filling varieties in sandstones often occur as dense, fine-grained aggregates (fig. 1*d*) which are difficult to distinguish optically from epidote or sphene. Vein-forming clinopyroxene crystallizes in distinctive spherulitic aggregates (fig. 3*c*) characterized by high extinction angles with respect to the elongation direction. Most authigenic clinopyroxenes in Cerro Prieto sandstones are colourless although greenish, slightly pleochroic varieties have been observed (e.g. in Well T366 at 2850 m). The Cerro Prieto pyroxenes (Table V) are all highly calcic augite, with M2 sites filled in excess of 90% by Ca. Molar Mg/(Mg + Fe + Mn) range from 0.23 to 0.90. Green clinopyroxenes in well T336 at 2850 m are the most hedenbergitic pyroxenes in the Cerro Prieto field. Colourless pyroxenes analysed from separate cuttings at the same depth interval are the most diopsidic (Table V).

Biotite is a minor phase ($< 5\%$ of the mode) in some sandstone cuttings from the higher temperature (i.e. > 300 °C) portion of the geothermal reservoir where it occurs in irregularly shaped to sub-spherulitic (fig. 3*f*) aggregates within the sandstone matrix and more rarely as coarser pseudomorphs of detrital phyllosilicates. The Cerro Prieto biotites are typically pale green to tan in colour. Representative compositions are presented in Table VI. Anhydrous oxide totals may range from 60 to 95%. Formula proportions in Table VI are recalculated using two methods (i.e. cation sum and cationic charge). Regardless of the method of recalculation, virtually all the Cerro Prieto biotites have low interlayer site occupancy and an interlayer charge < 0.85 cations/formula unit. Biotites from wells E2 and M123 have extremely low K contents, often as low as 0.25–0.30 per formula unit; these biotites have apparently crystallized as impure mixtures with another phyllosilicate phase characterized by K deficiency on the interlayer sites. The oxide analyses of these biotite mixtures, recalculated assuming a total cationic charge of +44 per formula unit (fig. 4), sheds some light on this unknown low-K, layer silicate. Unlike the cation sum method, the cationic charge method allows for octahedral cations (here arbitrarily chosen to be magnesium) to fill interlayer vacancies if the sum of octahedral Al + Fe + Mg + Mn exceeds 6.00 cations per formula unit. The potassium variation diagrams in fig. 4 show that although $Fe_{tot.}$ + Mg does not vary significantly with the K content, the interlayer Mg (Mg^{IL}, which is the octahedral excess of 6.00) systematically increases as the K content decreases, with a concomitant increase in Si. Unlike the biotite–vermiculite intergrowths described by McDowell and Elders (1980) from the Salton Sea geothermal system, the Ca content of the Cerro Prieto layer-silicate mixtures does not vary inversely with K. Although more detailed

TABLE IV. Compositions of actinolites from Cerro Prieto sandstones

Well	E2	E2	M53	M53	M73	M73	M93	M123
Depth(m)	1581	1680	1905	1935	1890	1890V	2424	1704
Temp(°C)	325	330	330	330	325?	325?	330	325?
	---Formula Proportions(1)---							
Si	7.99	8.06	8.01	8.05	7.91	7.80	7.88	8.05
Al^{IV}	0 01	0.00	0.00	0.00	0.09	0.20	0.12	0.00
Al^{VI}	0.23	0.18	0.15	0.04	0.12	0.02	0.15	0.25
Ti	bd	bd	0.00	0.02	bd	bd	0.01	bd
Fe	2.00	1.07	1.48	1.47	1.57	1.69	1.11	1.18
Mg	2.58	3.76	3.02	3.21	3.25	3.14	3.46	3.56
Mn	0.11	bd	0.34	0.25	0.13	0.16	0.11	0.07
Ca	2.08	1.92	2.00	1.96	1.93	1.98	2.15	1.90
Na	bd	bd	0.00	0.00	bd	bd	0.05	bd
K	bd	bd	0.04	0.03	bd	bd	0.01	bd
Total:	84.0	95.0	86.6	95.1	85.5	90.8	96.2	96.6
Method	eds	eds	wds	wds	eds	eds	wds	eds

(1) Formula proportions based on 15 cations exclusive of Na + K;

(2) Temperatures for wells M73 and M123 based on oxygen isotope geothermometry (Alan Williams, personal communications).

TABLE VI. Compositions of biotite and interlayered biotite/smectite (?) from Cerro Prieto sandstones

Well	E2	E2	M53	M53	M123	M125	M125
Depth(m)	1581	1680	1905	1935	1704	2310	2319
Temp(°C)	325	330	330	330	325?	335	335
Total	85.7	78.5	61.9	95.8	89.4	94.8	74.6
Method	eds	eds	eds	eds	eds	wds	wds
	---Formula Propositions = 7 cations - (Na + K + Ca)---						
Si	3.17	3.10	3.16	3.10	3.16	3.135	3.077
Al^{IV}	0.83	0.90	0.84	0.90	0.84	0.865	0.923
Al^{VI}	0.01	0.09	0.08	0.06	0.07	0.070	0.088
Ti	bd	bd	bd	0.01	bd	0.012	0.004
Fe	1.12	0.66	0.94	1.19	0.77	0.666	0.782
Mn	0.04	bd	0.06	0.02	bd	0.007	0.017
Mg	1.83	2.25	1.92	1.72	2.16	2.245	2.109
Ca	0.05	0.06	0.03	bd	0.04	0.013	0.051
Na	bd	bd	0.04	0.01	bd	0.015	0.044
K	0.25	0.39	0.66	0.83	0.64	0.697	0.666
	---Formula Proportions = cationic charge of +22---						
Si	3.24	3.14			3.17	3.141	3.080
Al^{IV}	0.76	0.86			0.83	0.859	0.920
Al^{VI}	0.95	0.14			0.085	0.076	0.090
Ti	BD	BD			BD	0.011	0.006
Fe	1.145	0.665			0.77	0.667	0.781
Mn	0.04	BD			BD	0.007	0.017
Mg^{VI}	1.72	2.295			2.145	2.239	2.106
Mg^{IL}	0.15	0.09			0.025	0.010	0.005
Ca	0.055	0.06			0.035	0.012	0.051
Na	BD	BD			BD	0.015	0.045
K	0.26	0.395			0.64	0.698	0.663

Mg^{IL} = Interlayer Mg which is [Al^{VI} + Ti + Fe + Mn + total Mg] - 3.00

TABLE V: Compositions of clinopyroxenes from Cerro Prieto sandstones

Well	M73	M73	M84	M93	M125	T366	T366
Depth(m)	1890	1890V	1557	2424	2241	2850 G(1)	2850
Temp(°C)	325?	325?	340	330	340	320	320
SiO_2	48.7	49.8	51.78	49.81	51.33	50.23	54.17
TiO_2	bd	bd	0.14	0.07	0.10	0.07	0.15
Al_2O_3	0.7	1.3	1.86	2.23	1.59	1.97	2.98
FeO(2)	20.8	17.4	9.27	12.53	15.10	18.51	2.63
MnO	3.0	3.4	1.86	5.14	2.07	0.11	0.13
MgO	4.1	4.4	10.38	5.96	6.11	6.02	15.35
CaO	19.7	23.2	24.04	24.04	22.68	21.41	23.24
Na_2O	bd	bd	0.30	0.21	0.40	1.14	0.54
Total	97.0	99.5	99.63	99.99	99.38	99.46	99.19
T							
Si	2.02	1.99	1.969	1.946	2.016	1.963	1.989
Al^{IV}	0.00	0.01	0.031	0.054	0.000	0.037	0.011
M(1)							
Al^{VI}	0.03	0.06	0.052	0.049	0.074	0.054	0.118
Ti	0.00	0.00	0.004	0.002	0.003	0.002	0.004
Fe	0.72	0.58	0.295	0.410	0.496	0.592	0.037
Mn	0.00	0.11	0.060	0.170	0.069	0.000	0.000
Mg	0.25	0.26	0.588	0.347	0.358	0.351	0.840
M(2)							
Fe	0.00	0.00	0.000	0.000	0.000	0.013	0.044
Mn	0.11	0.01	0.000	0.000	0.000	0.003	0.004
Ca	0.87	0.99	0.979	1.007	0.954	0.897	0.914
Na	0.00	0.00	0.022	0.016	0.031	0.087	0.038

(1) G = green clinopyroxene (see text); (2) Total Fe as FeO; formula proportions based on 4 cations.

TABLE VII. Compositions of sphene and garnet from Cerro Prieto sandstones

	Sphene(1)			Garnet(2)
Well	E2	M53	M73	E2
Depth(m)	1581	1797	1890	1581
Temp(°C)	325	310	325?	325
SiO_2	31.1	32.1	30.5	36.5
TiO_2	34.5	25.0	34.2	0.7
Al_2O_3	3.4	10.2	4.5	10.1
Fe_2O_3(3)	0.3	0.2	0.5	16.9
MnO				0.8
MgO		0.6		
CaO	29.1	30.4	28.1	33.7
Anhydr.				
Total	98.4	98.5	97.8	98.7
Si	1.01	1.00	0.99	2.96
Al	0.13	0.37	0.17	0.96
Ti	0.84	0.59	0.84	0.04
Fe	0.01	0.01	0.01	1.03
Mn	0.00	0.00	0.00	0.06
Mg	0.00	0.03	0.00	0.00
Ca	1.01	1.01	0.98	2.93

(1) Sphene formula proportions based on 5 oxygens;

(2) Garnet formula proportions based on 12 oxygens;

(3) Total iron expressed as Fe_2O_3.

work is necessary to fully describe these phases, it appears that the Cerro Prieto biotites are intergrown with a trioctahedral, smectite-like layer silicate, as is indicated by their high silica-content and interlayer Mg (or perhaps Fe). If the trends depicted in fig. 4 are extrapolated to potassium = 0.0 cations per formula unit, the composition of this hypothetical smectite would be close to: $Mg_{0.4}Ca_{0.2}(Mg,Fe,Al)_6Al_{1.3}Si_{6.7}O_{20}(OH)_4$. No systematic variations in the composition of the Cerro

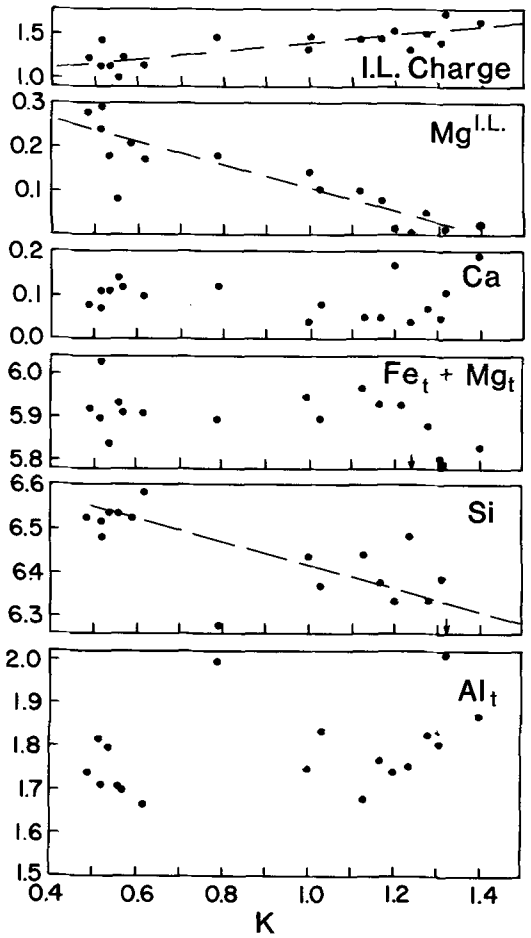

FIG. 4. Potassium variation diagrams for biotite–smectite(?) intergrowths from Cerro Prieto calcareous sandstones. Formula proportions calculated on the basis of a cationic charge of +44. Fe_t, Mg_t, and Al_t refer to the total proportions of these cations per formula unit. Mg^{IL} is the excess of $[6.00(Mg_t + Fe_t + Mn + Al^{VI})]$. See text for details.

Prieto biotites or biotite intergrowths were observed as a function of depth.

Sphene is a common accessory mineral in sandstones recovered from most depth and temperature intervals in the Cerro Prieto system. Authigenic sphene has been identified in sandstones which have probably not been recrystallized at temperatures exceeding 150 °C. Typically, sphene forms in very fine-grained xenoblastic aggregates in pore cements (fig. 2*e*), often intergrown with (and replacing?) detrital rutile. Sphene is a rare constituent of calc-silicate veins (fig. 3*a*). Representative analyses of Cerro Prieto sphenes are presented in Table VII. Cerro Prieto authigenic sphenes are distinctive in their extremely high Al_2O_3 contents, coupled with low Fe_2O_3. In this regard, they may be some of the most Al-rich authigenic sphenes that have been described (cf. Boles and Coombs, 1977).

Garnet is a rare but significant calc-silicate mineral in the Cerro Prieto geothermal system. The only documented garnet occurrence is in Well E2 at 1581 m (325 °C). In sandstone from this depth, idioblastic garnets (25–30 μm and comprising less than 1% of the mode) occur in a porous biotite + actinolite + sphene matrix which is incompletely cemented with epidote (fig. 3*e*). The composition of this garnet is presented in Table VII. It is a grandite with minor Ti and Mn. Compositional zoning and grain to grain variation of garnets in this sandstone are insignificant. The Cerro Prieto garnet is distinctly more aluminous than garnets from other active geothermal systems (reviewed by Bird *et al.*, 1984) and apparently one of the few that is in equilibrium with coexisting epidote (as described below).

Other hydrothermal minerals associated with those described above include quartz, chlorite, sericite (i.e. all dioctahedral colourless layer silicates), pyrite and chalcopyrite. Quartz modal abundances in the calc-silicate zone do not vary significantly from their detrital values, although dissolution and overgrowth features (often with pronounced fluid and solid inclusion trails) are common within many detrital grains (figs. 2 and 3). Chlorite and sericite have been identified in X-ray diffraction analyses and are most abundant (but generally $\ll 10\%$ of the bulk mode) in sandstones recrystallized below 300 °C. Wispy crystallites (e.g. fig. 3*d*) common to the pore spaces of many sandstones at all grades, yet too fine for microbeam analysis, may be chlorite, sericite, or actinolite. Pyrite and chalcopyrite (fig. 2*e*) are rare in Cerro Prieto calc-silicate assemblages. Lignite and vitrinite macerals (fig. 2*f*) are relatively common, especially in the finer-grained sediments. Barker and Elders (1981) report that vitrinite reflectance for phytoclasts in well M84 increases from 0.5 to 4.0 over the temperature interval of 50–350 °C.

Chemical equilibrium in the Cerro Prieto geothermal system

The Cerro Prieto geothermal system is a relatively youthful thermal anomaly, perhaps only 10^4 years old (Elders *et al.*, 1984). The consistent system-wide correlation between calc-silicate isograds and isotherms indicates that mineralogic equilibrium has been attained at least on a regional scale (Schiffman *et al.*, 1984). Authigenic and metamorphic mineral assemblages recrystallized between 150 and 350 °C are depicted in the ACF diagrams of fig. 5.

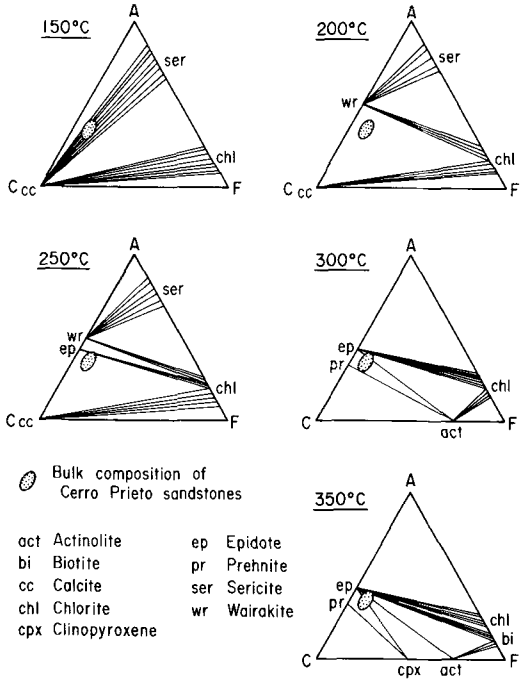

FIG. 5. $A(Al_2O_3+Fe_2O_3)$–$C(CaO)$–$F(FeO+MgO+MnO)$ diagrams for hydrothermally metamorphosed calcareous sandstones from the Cerro Prieto geothermal field at temperatures between 150 and 350 °C (Schiffman *et al.*, 1984).

Note that all assemblages in these diagrams also contain quartz + microcline ± sphene ± pyrite ± chalcopyrite ± organic material. Although most of the two and three phase assemblages denoted in fig. 5 have been observed petrographically or inferred by X-ray diffraction analysis, the critical univariant assemblages are distinctly rare and therefore the isogradal reactions are only poorly understood (Schiffman *et al.*, 1984). Bulk compositional changes in Cerro Prieto calcareous sandstones produced during hydrothermal recrystallization are as yet uninvestigated.

The distribution of octahedral cations amongst coexisting phases offers some indication of the degree to which the recrystallization of calcareous sandstones in the Cerro Prieto geothermal system has approached chemical equilibrium on the microscopic level. Partitioning of octahedral ferrous iron and magnesium between five coexisting actinolite–biotite pairs and three coexisting actinolite–clinopyroxene pairs is presented in fig. 6. The data points plotted on this diagram represent averages of several analyses from a given drill cutting of sandstone; 'coexisting' therefore implies that any two analysed grains were not physically separated by more than 2 or 3 mm. Representative mineral analyses for data plotted in fig. 6 are presented in Tables IV–VI. Note that all iron is considered as ferrous; recalculation of amphibole and clinopyroxene structure formulae using the methods described by Robinson (1980) and Robinson *et al.* (1982) indicates that ferric iron is rarely present which is consistent with the reducing conditions calculated for the geothermal reservoir (see below).

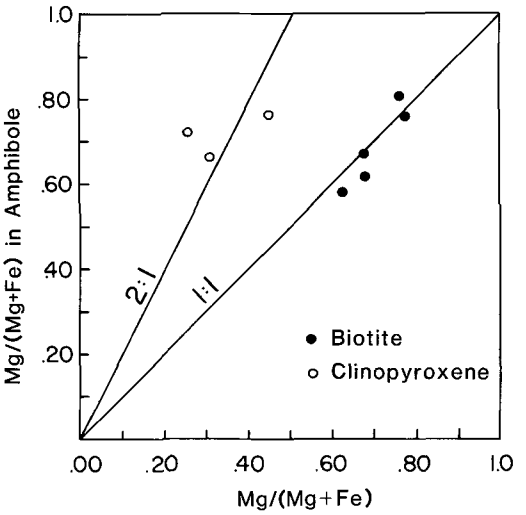

FIG. 6. Compositional relations between coexisting actinolite and biotite pairs (closed symbols) and coexisting actinolite and clinopyroxene pairs (open symbols) in Cerro Prieto calcareous sandstones. Mg/(Mg+Fe) denotes the mole fraction of octahedral Mg in actinolite, biotite, or clinopyroxene.

The ratios of the mole fraction of octahedral magnesium in actinolite to that in biotite are uniformly close to one (fig. 6). This is consistent with data from many calc-silicate metamorphic rocks (e.g. Hewitt, 1973; Rice, 1977; Keskinen, 1981) in which phlogopitic biotite and tremolitic-actinolite bearing assemblages occur over a wide temperature interval in the greenschist and amphibolite facies. The ratio of the octahedral mole fraction of magnesium in actinolite to that in coexisting clinopyroxene from Cerro Prieto calcareous sandstones is closer to 2:1 (fig. 6). This is significantly different to ratios determined in amphibolite facies rocks (e.g. Mueller, 1961; Hewitt, 1973; Rice, 1977; Kretz and Jen, 1978) which are close to unity. This disparity indicates that Cerro Prieto actinolite and clinopyroxene have not attained thermodynamic equilibrium, or that the

intercrystalline exchange equilibria between actinolite and clinopyroxene in geothermal environments is significantly different from that in amphibolite facies rocks.

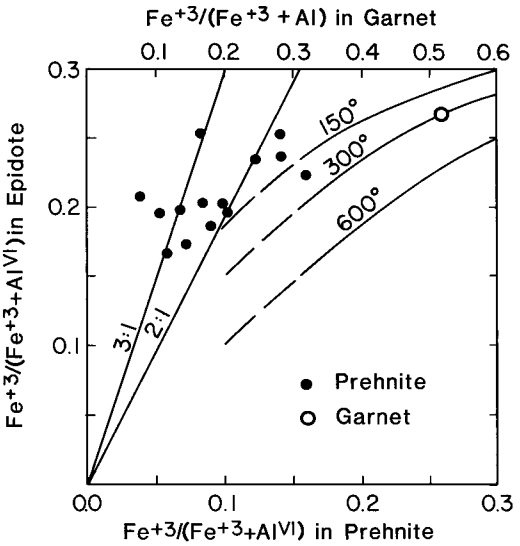

FIG. 7. Measured compositions of coexisting epidote–prehnite pairs (closed symbols) and epidote–garnet pair (open symbols) in Cerro Prieto calcareous sandstones. $Fe^{3+}/(Fe^{3+} + Al)$ denotes the mole fraction of octrahedral ferric iron in epidote (abscissa), garnet (top axis), or prehnite (bottom axis). The 150, 300, and 600 °C equilibrium partitioning isotherms for epidote–garnet are from Bird and Helgeson (1980).

Measured compositions of coexisting epidote and prehnite pairs and epidote and garnet pairs are depicted in fig. 7; representative mineral analyses are given in Tables III and VII. The ratio of octahedral site mole fraction of total ferric iron in epidote to that in prehnite from Cerro Prieto calcareous sandstones ranges from approximately 1.5/1 to 4/1 for values of $X_{Ca_2Fe_3Si_3O_{12}(OH)}$ between 0.15 and 0.25. This is consistent with experimental data and natural paragenesis (Liou *et al.*, 1983) which indicate that octahedral site mole fraction of total ferric iron in epidote is typically 1.5 to 8 times greater than that in coexisting prehnite of the prehnite–pumpellyite or greenschist facies. Partitioning of octahedral ferric iron and aluminium between coexisting grandite garnet and epidote and its use as a geothermometer in calc-silicate assemblages such as skarns, has been presented by Bird and Helgeson (1980). The compositions of coexisting epidote and garnet from well E2 at 1581 m (Tables III and VII) are consistent with the calculated 300 °C isotherm for equilibrium Fe^{3+}/Al^{VI} partitioning and is in excellent agreement with a downhole temperature measurement of 325 °C. A review of the compositional relations of garnet and epidote from other active geothermal systems (e.g. Larderello, Salton Sea, and the Geysers systems) by Bird *et al.* (1984) indicates that equilibrium partitioning of octahedral ferric iron and aluminium in these phases is rarely attained in active geothermal systems.

Thermodynamic analyses of phase relations among calc-silicate mineral assemblages and interstitial fluids from the Cerro Prieto geothermal system have been presented by Bird *et al.* (1984). In that study it is shown that epidote and prehnite assemblages buffer the logarithmic activity ratio of $(a_{Ca^{2+}}/a^2_{H^+})$ in the fluid phase to values between 7.0 and 7.5, but for epidote and clinopyroxene assemblages the range of values is larger and between 6.5 to 8.5. Assuming local equilibrium for the epidote and clinopyroxene assemblages allows calculation of the logarithm of the activity ratio of Ca^{2+} to Mg^{2+} in the fluid buffered by this assemblage. Calculations presented by Bird *et al.* (1984) and shown in fig. 8*a* illustrate that the logarithm of $(a_{Ca^{2+}}/a^2_{Mg^{2+}})$ ranges from 2.5 to 4.5, which is in close agreement with measured molarity ratios in high-temperature reservoir fluids (Fausto *et al.*, 1979) of $\log(m_{Ca^{2+}}/m_{Mg^{2+}})$ between 2.5 and 3.5 (see fig. 8*a*). These calculations have also demonstrated that the conditions of formation of pore-filling epidote and clinopyroxene cementation of the Cerro Prieto sands requires extremely reducing conditions close to or below the quartz–fayalite–magnetite buffer (fig. 8*b*) and that the logarithm of the oxygen fugacity is nearly a linear function of the composition of the epidote pore-filling cement (fig. 8*c*).

Similar types of calculations for the pyroxene-absent assemblage of garnet, epidote, actinolite, quartz, and microcline ($X_{KAlSi_3O_8} = 0.94$) found in well E2 at 1.58 km depth and approximately 325 °C allows for simultaneous evaluation of the thermodynamic activity ratios of $a_{Ca^{2+}}/a^2_{H^+}$, $a_{Mg^{2+}}/a^2_{H^+}$, a_{K^+}/a_{H^+}, $a_{Fe^{3+}}/a^2_{H^+}$, $a_{Fe^{2+}}/a^2_{H^+}$, and $a_{Al^{3+}}/a^3_{H^+}$, together with the activity of SiO_2 (aqueous) and the fugacity of oxygen in the fluid phase consistent with local equilibrium among these minerals and the interstitial fluids. Activity–composition relations and data sources employed in these calculations are summarized in Bird and Norton (1981) and Bird *et al.* (1984), and the results of the calculations are illustrated in figs. 8 and 9 for the compositions of coexisting epidote, garnet, and biotite given in Tables III, VI, and VII.

It can be seen from the phase diagrams in fig. 9 that the assemblage of garnet, epidote, biotite,

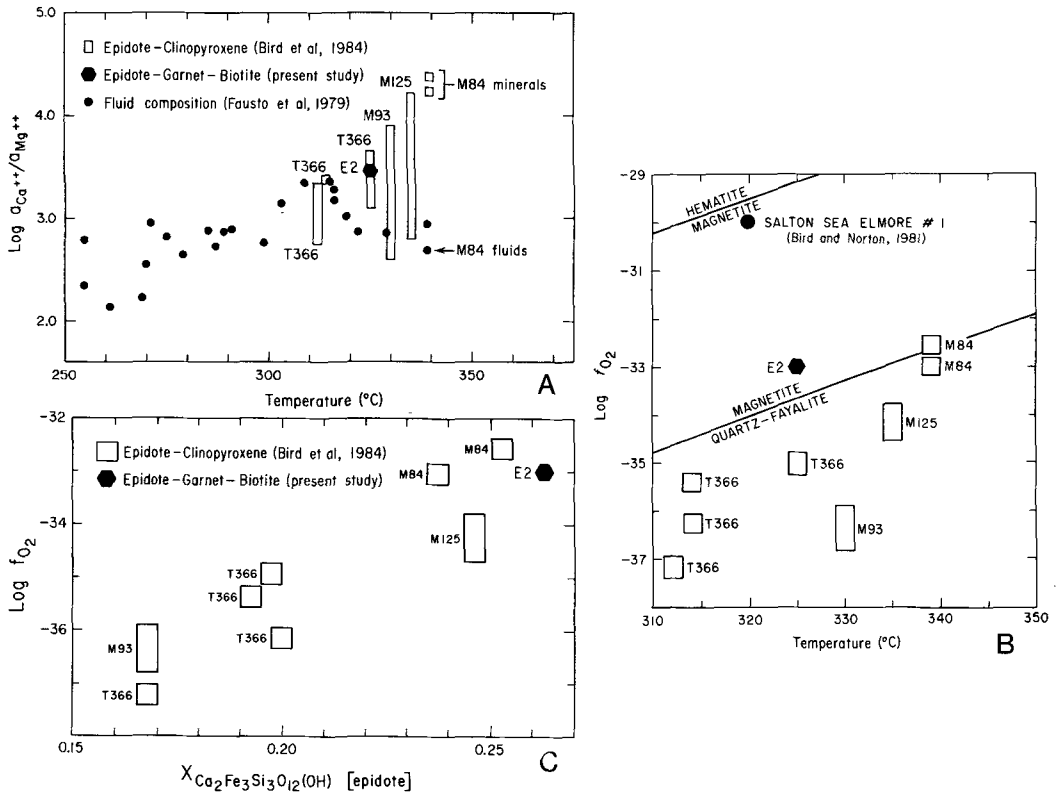

FIG. 8. Predicted values of $a_{Ca^{2+}}/a_{Mg^{2+}}$ (*a*) and fugacity of oxygen (*b*, *c*) in geothermal fluids that are in local equilibrium with epidote and clinopyroxene mineral assemblages (open symbols) or epidote and garnet mineral assemblages (solid hexagon) from sandstones in the Cerro Prieto geothermal system (modified from Bird *et al.*, 1984). Predicted values are calculated using equations and data reported by Helgeson and Kirkham (1974*a*, *b* and 1976), Helgeson *et al.* (1978, 1981), Walther and Helgeson (1977), Bird and Helgeson (1980), and Bird and Norton (1981). Solid circles in (*a*) denote measured ratios of the molality of total calcium to total magnesium in geothermal fluids from Cerro Prieto reported by Fausto *et al.* (1979). See text for details.

microcline, quartz, and an aqueous solution, buffers the cation to hydrogen ion activity ratios in the coexisting fluid to: $\log(a_{Ca^{2+}}/a_{H^+}^2) = 7.5$, $\log(a_{K^+}/a_{H^+}) = 4.35$, and $\log(a_{Mg^{2+}}/a_{H^+}^2) = 4.0$. Note in fig. 9*b* that this fluid is slightly supersaturated with respect to tremolite. This is most likely due to the consequences of interlayer site vacancies in the biotite (as previously described) that were not accounted for in the present calculations. If considered, the biotite stability field and the $\log(a_{Mg^{2+}}/a_{H^+}^2)$ in the fluid phase would be lowered to a value closer to that of tremolite saturation. This trend is consistent with heterogeneous equilibrium among biotite, tremolite, and an aqueous solution, as also indicated by the octahedral partitioning of magnesium and ferrous iron amongst these phases (see fig. 6). The calculated value of $\log(a_{Ca^{2+}}/a_{Mg^{2+}})$ for the epidote-garnet bearing assemblage is approximately 3.5 overlapping the prediction of Bird *et al.* (1984) for fluids in local equilibrium with epidote and clinopyroxene assemblages from Cerro Prieto at similar temperatures in well T366 (see fig. 8*a*).

The calculations presented above together with the law of mass action for the reaction:

$$\begin{array}{ccc} 4Ca_2FeAl_2Si_3O_{12}(OH) & & 4KFe_3(AlSi_3O_{10})(OH)_2 \\ \text{(in epidote)} & & \text{(in biotite)} \\ + & & + \\ 4Ca_3Fe_2Si_3O_{12} & \longrightarrow & 2Ca_3Al_2Si_3O_{12} \\ \text{(in garnet)} & \longleftarrow & \text{(in garnet)} \\ + & & + \\ 4K^+ + 4H^+ & & 6SiO_2 + 10H_2O + 3O_2 \\ \text{(in aqueous solution)} & & \text{(quartz)}\quad \text{(water)}\quad \text{(gas)} \end{array}$$

allows calculation of the fugacity of oxygen consistent with local equilibrium among the assemblage of minerals represented in fig. 9 for well E2 at 1.58 km depth. The results are represented by the

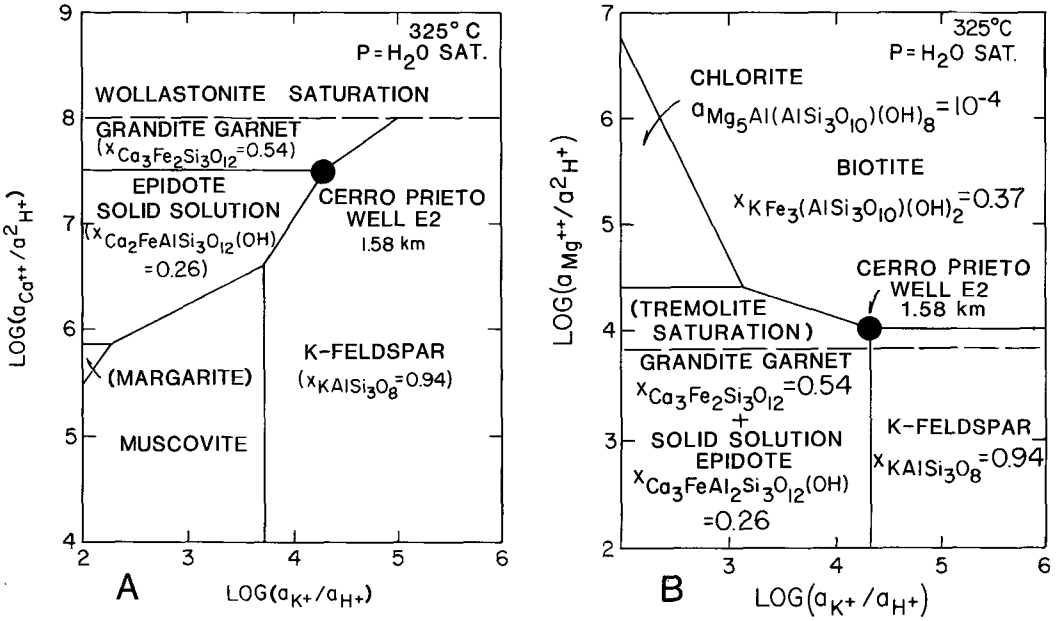

FIG. 9. Logarithmic activity-activity phase diagrams for the system K_2O-CaO-MgO-Fe_2O_3-FeO-Al_2O_3-SiO_2-H_2O-HCl at 325 °C and liquid-vapour equilibrium for pure H_2O in equilibrium with quartz (see fig. 8 caption for references). Solid symbol denotes the calculated activity ratios of $a_{Ca^{2+}}/a^2_{H^+}$ (fig. 9*a*) and $a_{Mg^{2+}}/a^2H^+$ versus a_{K^+}/a_{H^+} (fig. 9*b*) in the interstitial fluids equilibrated with epidote, garnet, biotite, microcline, quartz, and an aqueous solution. See Tables III, VI, and VII for mineral analysis.

solid hexagon in fig. 8*b* and *c* as a function of the measured downhole temperature and of the composition of epidote in the garnet bearing assemblage. Note in fig. 8*c* the near linear relationship of $\log f_{O_2}$–$X_{Ca_2Fe_3Si_3O_{12}(OH)}$. In contrast to this relationship and the similarity in $a_{Ca^{2+}}/a_{Mg^{2+}}$ ratio in the fluid phase for the epidote-garnet and epidote-clinopyroxene assemblages shown in fig. 8*a*, the fugacity of oxygen for the garnet-bearing assemblages is about two orders of magnitude lower than that predicted for the clinopyroxene assemblages at 325 °C as shown in fig. 8*b*. These relationships illustrate that although major cation activity ratios in the interstitial fluid may be relatively insensitive to phase relations among iron-bearing hydrothermal minerals, the oxygen fugacity is apparently not and can vary considerably (at constant temperature) within this geothermal system.

Fugacities of oxygen in equilibrium with epidote and clinopyroxene in high temperature Cerro Prieto fluids are about five orders of magnitude more reducing (i.e. 10^{-35} versus 10^{-30}) than those in the Salton Sea geothermal fluid (fig. 8*b*). The relatively low ferric iron contents of epidotes, the absence of hematite, and the abundance of organic material all attest to the highly reducing nature of Cerro Prieto fluids. H_2O and CH_4 may be the dominant gas species in equilibrium with pyroxene-bearing calc-silicate assemblages. The ubiquitous assemblage of sphene + quartz + calcite ± rutile buffers X_{CO_2} for fluids in equilibrium with Cerro Prieto calc-silicate assemblages to exceedingly small values.

Acknowledgements. The research described above was supported by the US Department of Energy contract no. DE-FC07-80ID12145. This is report No. UCR-IGPP 8424 of the Institute of Geophysics and Planetary Physics, University of California, Riverside. We thank our colleagues at the University of California, Riverside, Lawrence Berkeley Laboratory, and La Comisión Federal de Electricidad for their assistance and co-operation during our studies at Cerro Prieto. Our thanks to James Hoagland and Doug McDowell who collected some of the microprobe analyses used in this study, and to Doug Robinson and an anonymous reviewer whose comments have materially improved this manuscript.

REFERENCES

Albee, A. L., and Ray, L. (1970) *Anal. Chem.* **42,** 1409–14.

Barker, C. E., and Elders, W. A. (1981) *Geothermics*, **10,** 207–23.

Bence, A. E., and Albee, A. L. (1968) *J. Geol.* **76,** 382–406.

Bird, D. K., and Helgeson, H. C. (1980) *Am. J. Sci.* **280,** 907–41.
——and Norton, D. L. (1981) *Geochim. Cosmochim. Acta,* **45,** 1479–93.
——Schiffman, P., Elders, W. A., Williams, A. E., and McDowell, S. D. (1984) *Econ. Geol.* **70,** 671–95.
Boles, J. R., and Coombs, D. S. (1977) *Am. J. Sci.* **277,** 982–1012.
Bowen, N. L. (1940) *J. Geol.* **48,** 225–74.
Colby, J. W. (1968) *Advances in X-ray Analysis* II, 287–305.
Elders, W. A., Hoagland, J. E., McDowell, S. D., and Cobo, J. M. (1979) *Geothermics,* **8,** 201–5.
—— Bird, D. K., Williams, A. E., and Schiffman, P. (1984) **13,** 27–47.
Fausto, J. J., Sanchez, A., Jimenez, M. E., Esquar, I., and Ulloa, F. (1979) *LBL Rep.* 1197, 188–220.
Fuis, G. S., Mooney, W. D., Healy, J. H., McMechan, G. A., and Lutter, W. J. (1982) *U.S.G.S. Prof. Paper,* 1254, 25–50.
Harker, A. (1932) *Metamorphism,* Methuen, London. 362 pp.
Helgeson, H. C., and Kirkham, D. H. (1974*a*) *Am. J. Sci.* **274,** 1089–198.
————(1974*b*) Ibid. **274,** 1198–261.
————(1976) Ibid. **276,** 97–240.
——Delany, J. M., Nesbitt, H. W., and Bird, D. K. (1978) Ibid. **278-A,** 229 pp.
——Kirkham, D. H., and Flowers, G. C. (1981) Ibid. **281,** 1249–516.
Hewitt, D. A. (1973) Ibid. **273-A,** 444–69.
Keskinen, M. (1981) Ibid. **281,** 896–921.
Kretz, R., and Jen, L. S. (1978) *Can. Mineral.* **16,** 533–7.
Liou, J. G., Kim, H. S., and Maruyama, S. (1983) *J. Petrol.* **24,** 321–42.
McDowell, S. D., and Elders, W. A. (1980) *Contrib. Mineral. Petrol.* **74,** 293–310.
Mueller, R. F. (1961) *Geochim. Cosmochim. Acta,* **25,** 267–96.
Muffler, L. P. J., and Doe, B. (1968) *J. Sediment. Petrol.* **38,** 384–99.
——and White, D. E. (1969) *Geol. Soc. Am. Bull.* **80,** 157–82.
Rice, J. M. (1977) *Am. J. Sci.* **277,** 1–24.
——and Ferry (1982) *Rev. Mineral.* **10,** 263–326.
Robinson, P. (1980) *Rev. Mineral.* **7,** 419–94.
——Spear, F. S., Schumacher, J. C., Laird, J., Klein, C., Evans, B. W., and Doolan, B. L. (1982) *Rev. Mineral.* **9B,** 1–228.
Schiffman, P., Elders, W. A., Williams, A. E., McDowell, S. D., and Bird, D. K. (1984) *Geology,* **12,** 12–15.
Scholle, P. A., and Schluger, P. R. (eds.) (1979) *Aspects of Diagenesis,* S.E.P.M. Spec. Publ. No. 26.
Van de Kamp, P. C. (1973) *Geol. Soc. Am. Bull.* **84,** 827–48.
Walther, J. V., and Helgeson, H. C. (1977) *Am. J. Sci.* **277,** 1315–51.

[*Manuscript received 13 April 1984; revised 26 October 1984*]